

COMPUTATION AND EVALUATION OF WALL SHEAR STRESS DISTRIBUTION AT THE LOWER SURFACE OF A RADIAL FLOW CELL

J. G. Detry¹, B. B. B. Jensen², C. Deroanne¹ and M. Sindic¹

¹ Food Technology Department, Gembloux Agricultural University, Passage des Déportés, 2, 5030 Gembloux, Belgium.
E-mail: detry.j@fsagx.ac.be

² Department of Food Process Engineering, BioCentrum-DTU, Technical University of Denmark, Soltofts Plads Building 221, 2800 Lyngby, Denmark. E-mail: bbb@biocentrum.dtu.dk

ABSTRACT

In the present work, the flow in the radial-flow cell was analyzed for an aspect ratio of 1 with inlet pipe Reynolds numbers of 950, 2 000 and 4 100. Two models were applied to compute the wall shear stress distribution at the lower surface, at any distance from the center. Stainless steel and polystyrene surfaces were soiled with oil and starch and the detachment of these soils was assessed by measuring the detachment radius in a radial-flow cell. The experimental radii were introduced in the models and converted into wall shear stress. Comparisons of the various sets of data suggest that soil removal was not controlled by wall shear stress alone. Satisfactory estimations of the wall shear stress could be obtained at low radial positions for laminar flow, pointing out the usefulness of CFD for the computation of the critical wall shear stress when soil removal occurs in this region.

INTRODUCTION

The removal of soils from solid surfaces is a daily problem in the food industry, in medical applications and in the catering industry where hygiene is a constant concern. In the case of open surfaces like wall-panels in cold storage rooms, splashing can occur during food products handling, leading to surface soiling. Such soiled surfaces constitute a potential source of contamination and a favorable environment for microbial proliferation. Their cleaning is thus essential to ensure the quality of the products.

Wall shear stress is known to play an important role in the removal of soils from solid surfaces exposed to a liquid flow parallel to the surface (Jensen, 2003). The application of systems generating this kind of flow is frequently reported in microbial adhesion studies (Boonaert et al., 2002). One of those systems, the radial-flow cell (RFC), has been used very recently to assess the removal of various soils from solid surfaces, showing the influence of wall shear stress on soil removal (Jensen and Friis, 2004; Detry et al., 2007).

The principle of the RFC is illustrated in Figure 1. It consists of two parallel disks with a narrow spacing in-

between. The cleaning fluid exits the center of one disk at a constant volumetric flow rate and flows radially outward between the disks. As the cross-sectional area between the disks increases with the radial position, the linear fluid velocity and hence the shear stress near the surface decrease radially across the disk, submitting the adherent soils to a continuous range of shear forces in one experiment. This is advantageous with respect to applying a sequence of shear rates using a parallel plate flow chamber because it allows kinetic runs to be performed in a shorter time (Bakker et al., 2002).

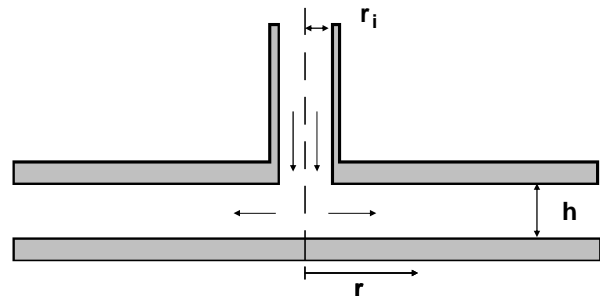


Fig. 1: Principle of the radial flow cell

However, the hydrodynamics of the system are complex due to the geometry of the inlet. The exact relation between the detachment radius and the surface shear stress is not yet totally clarified (Goldstein and DiMilla, 1997; Klavenes et al., 2002; Jensen and Friis, 2004). At larger radial positions, analytical and empirical models for ideal laminar or turbulent flow diverging between two parallel discs can be applied (fully developed velocity profile originating from the symmetry axis of the RFC) because the inlet geometry no longer affects the flow (Fryer et al., 1985; Jensen and Friis, 2004). At low radii, these models cannot be used and numerical solutions must be applied (Goldstein and DiMilla, 1997).

In previous work, the detachment of oil droplets from model substrates was studied in the RFC (Detry et al., 2007). However, oil removal occurred in the zone where the flow conditions are not well defined, preventing the application of the analytical models available to convert the detachment radius measured at the sample surface into wall shear stress. This reduces the potential of the RFC to provide a wide range of wall shear stress values associated to the detachment radius in one experimental setup. Consequently, the ability of commercial CFD codes to give a quantitative distribution of the wall shear stress at any radial position of the sample surface can be of particular interest to both materials and equipment manufacturers. It allows the determination of high critical wall shear stresses required for soil removal on different substrates as well as absolute comparisons between them in terms of cleanability.

The aim of the present work is the determination of the critical wall shear stress required for soil removal and of its dependency toward the flow rate. If soil removal is controlled by wall shear stress alone, then the critical wall shear stress should be independent from the flow rate.

MATERIAL AND METHODS

Surfaces Pretreatment

Before soiling, the polystyrene (50 x 50 x 0.25 mm – Goodfellow, United-Kingdom) and stainless steel (50 x 50 x 1 mm – Arcelor, France) samples were immersed in 200 ml ethanol 96 % for 10 min. The samples were then dried with Kimtech Science paper (Kimberly–Clark, United Kingdom) and immersed for 10 min at 50 °C in an alkaline detergent solution (RBS 50 from Chemical Products) at a concentration of 2 % (v/v) (pH = 11.9). The surfaces were then rinsed five times in 200 ml water (MilliQ-50 system – Millipore, France) at 50 °C, five times in 200 ml water at room temperature and dried with a gentle flow of nitrogen. An additional UV treatment (40 min at 254 nm) was performed on stainless steel plates to improve the removal of organic contamination; the plates were then wrapped in aluminum foil until soiling.

Soiling Procedure

The surfaces were soiled with commercial edible sunflower oil from Carrefour (Belgium) or with an aqueous suspension of waxy corn starch granules (20 % w/v) from Sigma. The oil was stained with β -carotene (0.01 % w/w) and the starch with sodium fluoresceinate (0.02 % w/v). Soiling was performed by manual aspersion using a thin layer chromatography (TLC) sprayer located at 40 cm from the surface. Oil-soiled surfaces were used directly in the flow cell whereas starch-soiled surfaces were dried for 30 min in

darkness at room temperature before use. Pictures of each starch-soiled surface were taken with a ZX9 stereomicroscope (Olympus – Belgium) in epifluorescence equipped with a CCD camera, a mercury vapor UV lamp (100 W, emission range 100 – 800 nm) and UV filters (passing bands: excitation 460 – 490 nm, emission > 520 nm).

Cleanability Assessment

Radial-flow cell: The radial-flow cell is made of stainless steel. It consisted of an upper disk with a 2 mm – diameter central inlet and a lower disk in which the soiled square sample was put. A trench was made along the perimeter of the square recess in the lower disk to avoid any perturbation generated by deformations of the sample near the cut edges. The distance (h) between the upper disk and both the sample and the lower disk was set by three adjustable micrometric screws and controlled to be 1.00 ± 0.02 mm with calibrated steel spacers. The fluid entering the cell was pumped from a 10 liter tank by a peristaltic pump (Watson Marlow 323SciQ, pumphead 314, 4 rollers). Before entering the cell, the fluid passed through a surge tank to reduce the pulses from the pump.

Sunflower oil: The cleaning fluid was a solution of commercial detergent (Monsieur Propre – Procter & Gamble, France) at a concentration of 1.2 % (v/v) which was higher than the critical micellar concentration (pH = 8.2). The surface tension of the solution was $27.1 \text{ mN}\cdot\text{m}^{-1}$.

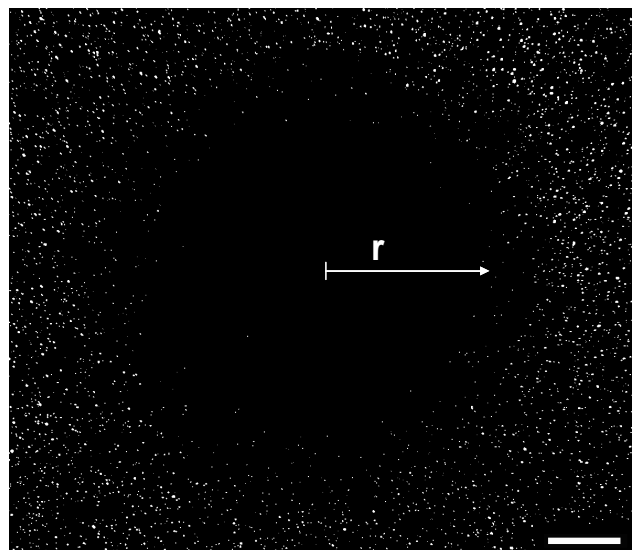


Fig. 2: Central cleaned zone on a starch-soiled polystyrene surface submitted 5 min to a flow rate of $390 \text{ ml}\cdot\text{min}^{-1}$ in the RFC (Scale bar: 3 mm).

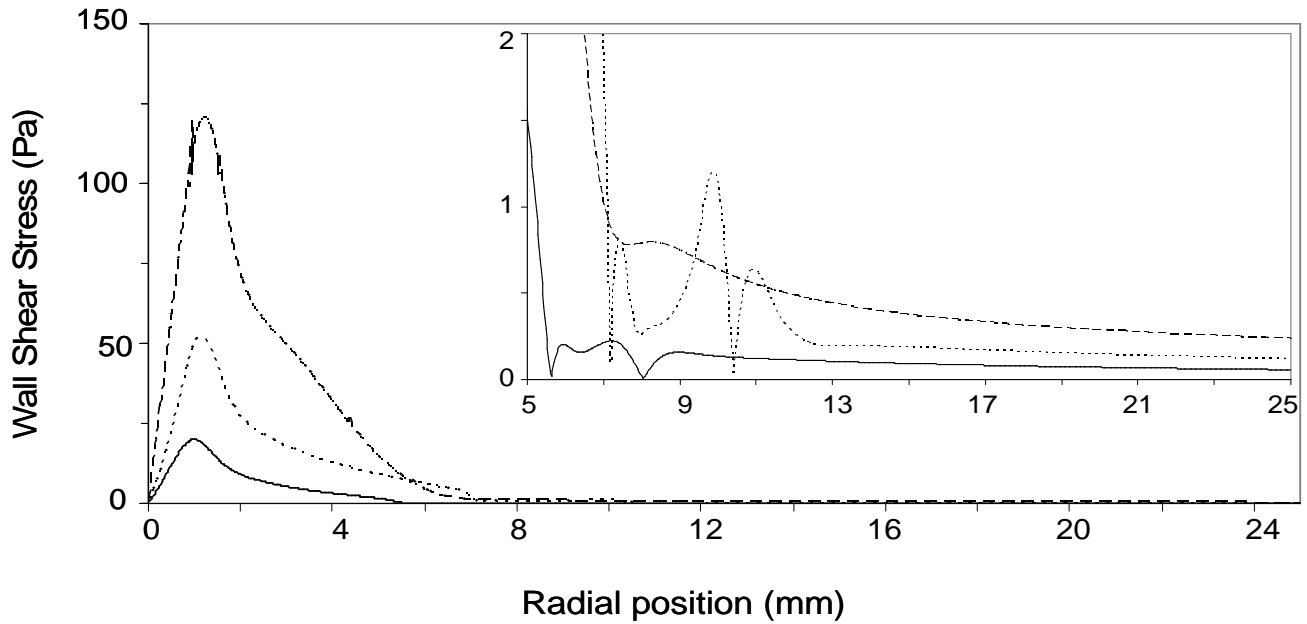


Fig. 3: Wall shear stress distribution at the lower wall of the RFC for inlet flow rates of 90 ml.min⁻¹ (—), 190 ml.min⁻¹ (.....) and 390 ml.min⁻¹ (- - - -). The small graph in the upper right corner presents an enlargement of the distribution for radial positions > 5 mm.

(TVT1 – LAUDA, Germany). The cleaning sequences were performed at 20 °C and at two flow rates (190 ml.min⁻¹ and 390 ml.min⁻¹) for different periods of time (30 s; 1, 2, 3, 5, 7, 10 and 15 min). After cleaning, the sample was removed and the diameter of the circle exempt of oil was measured using a caliper or the ZX9 stereomicroscope. The LUCIA G image analysis software was coupled to the CCD camera of the stereomicroscope to determine the detachment radius (*r*). The experiments were performed in triplicate.

Starch granules: The cleaning fluid was water and the cleaning sequences were performed at 20 °C at three flow rates (90 ml.min⁻¹, 190 ml.min⁻¹ and 390 ml.min⁻¹) for 5 min. After cleaning, the sample was removed. The detachment radius was not as sharp as for oil and pictures of the circular zone containing a lower density of deposits were taken with the ZX9 stereomicroscope in epifluorescence (Figure 2). The pictures were then processed with a specific application of the Matlab (The Mathworks Inc.) software which gives the ratio of the number of aggregates before and after cleaning according to the radial position. A graph could then be plotted to determine the radial positions corresponding to residual densities of deposits of 5 %, 10 %, 20 %, 30 %, 40 % and 50 %. To ensure repeatability, at least 10 repetitions of each experiment were performed in three independent series.

WALL SHEAR STRESS

Analytical Models

The local Reynolds number between the disks and the Reynolds number in the inlet pipe are given by Eq. (1) and (2), respectively (Moller, 1963):

$$Re_r = \frac{\rho \cdot Q}{\pi \cdot \mu \cdot r} \tag{1}$$

$$Re_{inlet} = \frac{2 \cdot \rho \cdot Q}{\pi \cdot \mu \cdot r_i} \tag{2}$$

where ρ is the density of the fluid, Q is the volumetric flow rate, μ is the dynamic viscosity, r_i the radius of the inlet pipe and r the radial position from the inlet.

The wall shear stress (Pa) for the creeping flow of an incompressible Newtonian fluid was defined by Moller (1963):

$$\tau = \frac{3 \cdot \mu \cdot Q}{\pi \cdot r \cdot h^2} \tag{3}$$

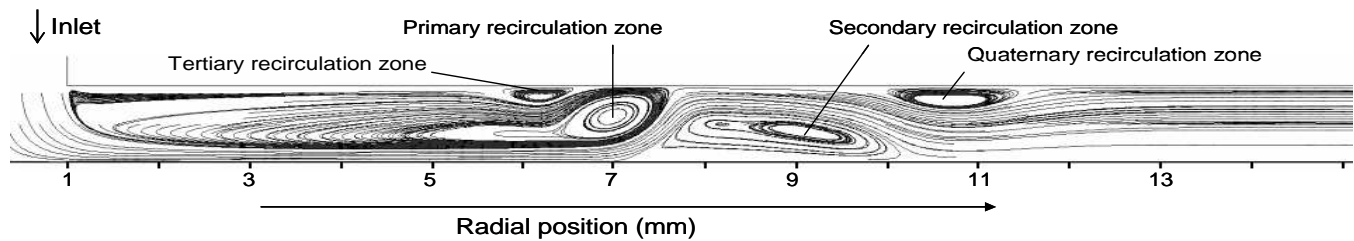


Fig. 4: Morphology of the flow in the radial flow cell at $190 \text{ ml}\cdot\text{min}^{-1}$ (Jensen et al., submitted)

This equation is valid as long as the inertial forces are small with respect to the viscous forces: the influence of the inlet geometry is no longer present and the flow is a fully developed decelerating flow. This condition can be expressed using a local modified Reynolds number (Fryer et al., 1985):

$$Re_{\text{modified}} = \frac{\rho Q}{24 \pi r \mu} \cdot \frac{h}{r} \leq 0.25 \quad (4)$$

An inertial correction can be introduced in Eq. (3) but its use seems also limited to low Reynolds number, when the effect of the inlet geometry is not too important (Goldstein and DiMilla, 1997; Klavenes et al., 2002).

CFD Models

Meshes were created in GAMBIT ver 2.2.30 (Fluent Inc.). Simulations were performed using Fluent ver 6.2.16 (Fluent Inc.). All meshing was done using quadratic hexahedral cells in a regular structured mesh. The Navier-Stokes equations were solved by the finite volume method. The simulations used the 2D axis symmetric solver and the SIMPLE algorithm was used to couple pressure and velocity. A detailed description of the CFD simulation and the relevancy of their solutions are given in Jensen et al. (submitted).

Wall shear stress distributions given by two CFD models were used in the present work (Figure 3). When the flow in the inlet was laminar ($Re_{\text{inlet}} \leq 2000$), the laminar model of Fluent was used with the power law discretization scheme and a uniform mesh of 88 000 cells. For turbulent flow in the inlet pipe ($Re_{\text{inlet}} \geq 4000$), the shear stress transport (SST) $k-\omega$ model for transitional flows was applied (with an inlet turbulent intensity of 10 % and a turbulent length scale equal to the hydraulic diameter of the RFC). The discretization scheme was the same as for laminar flow but additional mesh refinement of the near wall cells was performed by Fluent according to $y^+ < 1$.

In the case of the laminar model, mesh independence had been checked as well as the evolution of the flow pattern with the volumetric flow rate. At a flow rate of $90 \text{ ml}\cdot\text{min}^{-1}$ ($Re_{\text{inlet}} = 955$), two recirculation zones were observed: the

primary one due to the detachment of the flow from the upper wall at the inlet corner (between 1.0 and 6.1 mm) and the secondary one (between 5.6 and 8.1 mm). At $190 \text{ ml}\cdot\text{min}^{-1}$ ($Re_{\text{inlet}} = 2016$), three major recirculation zones were identified (the primary one between 1.0 and 7.8 mm; the secondary between 7.2 and 10.4 mm and the quaternary between 10.1 and 11.3 mm) and one smaller one, located within the primary one between 5.8 and 6.5 mm (Figure 4). This complex flow pattern is in good agreement with previous experimental studies performed in similar geometries (Armaly et al., 1983; Hsieh and Lin, 2005).

For turbulent flow in the inlet pipe, mesh independence was verified but mesh refinement according to $y^+ < 1$ induced an unavoidable sudden discontinuity in the y^+ curve at the considered flow rate ($390 \text{ ml}\cdot\text{min}^{-1}$, $Re_{\text{inlet}} = 4138$). This discontinuity was situated at a radial position of 4.5 mm and led to the apparition of irregularities in the wall shear stress distribution (Figure 3). The model predicted only one recirculation zone at the upper wall of the RFC for radial positions between 1.0 and 7.5 mm as expected from literature (Armaly et al., 1983).

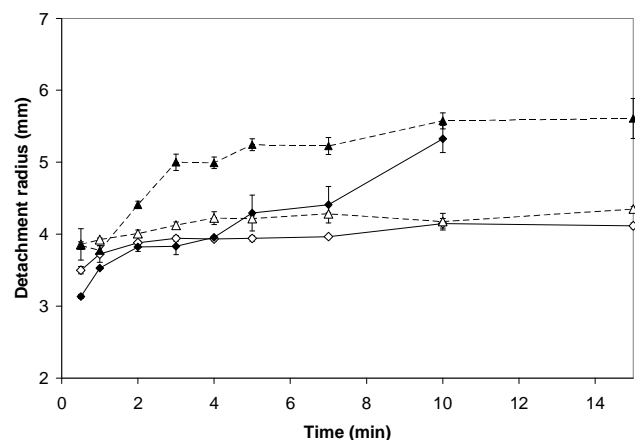


Fig. 5: Evolution of the detachment radius at flow rates of $190 \text{ ml}\cdot\text{min}^{-1}$ (—, \blacklozenge) and $390 \text{ ml}\cdot\text{min}^{-1}$ (---, \blacktriangle) for polystyrene (open symbols) and stainless steel (closed symbols) (Detry et al., 2007).

RESULTS

Sunflower Oil

The influence of the two cleaning flow rates on the evolution of the detachment radius was studied on stainless steel and polystyrene substrates. The results are shown in Figure 5. In the case of polystyrene, no difference in detachment radii was measured according to the flow rate. After a small initial increase, the detachment radius stabilized around about 4 mm. For stainless steel surfaces, the growth of the detachment radius was more discernible and the radius was larger at the higher flow rate. The differences between the two flow rates were more visible on this substrate. Eq. (3) was applied for converting the detachment radius measured on both substrates into wall shear stress as illustrated by Figure 6a. The figure presents, in principle, the

time evolution of the wall shear stress required to detach the oil drops, providing a detachment shear stress (about 1 Pa) that varies according to the flow rate. Wall shear stress values at the polystyrene and stainless steel surfaces were also deduced from CFD for the measured detachment radii as shown in Figure 7 and plotted as a function of cleaning time in Figure 6b.

The wall shear stress values given by the CFD models are more than 10 times those computed with Eq. (3). For polystyrene, the wall shear stresses varied by a factor of 2 between the flow rates whatever the cleaning time, as observed in Figure 6a using Eq. (3). For stainless steel, during the first minutes of cleaning, the wall shear stress values predicted by CFD at 390 ml.min⁻¹ drop from the values computed for polystyrene at the same flow rate to those obtained at 190 ml.min⁻¹. After 3 min of cleaning, the wall shear stress values were the same independently from

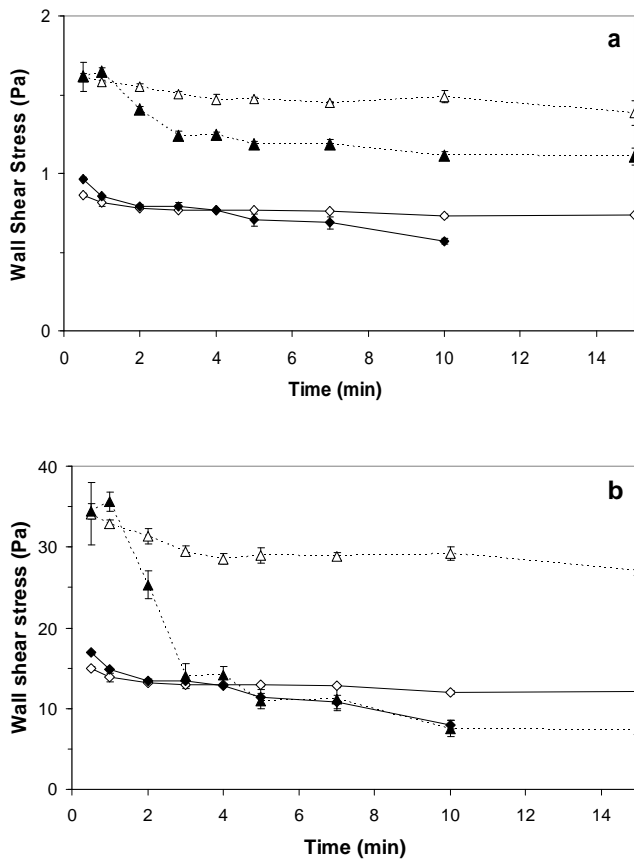


Fig. 6: Evolution of the wall shear stress corresponding to the detachment radii of Figure 5 for polystyrene (open symbols) and stainless steel (closed symbols) at flow rates of 190 ml.min⁻¹ (—, ♦) and 390 ml.min⁻¹ (---, ▲). Computations using (a) Eq. (3) and (b) CFD.

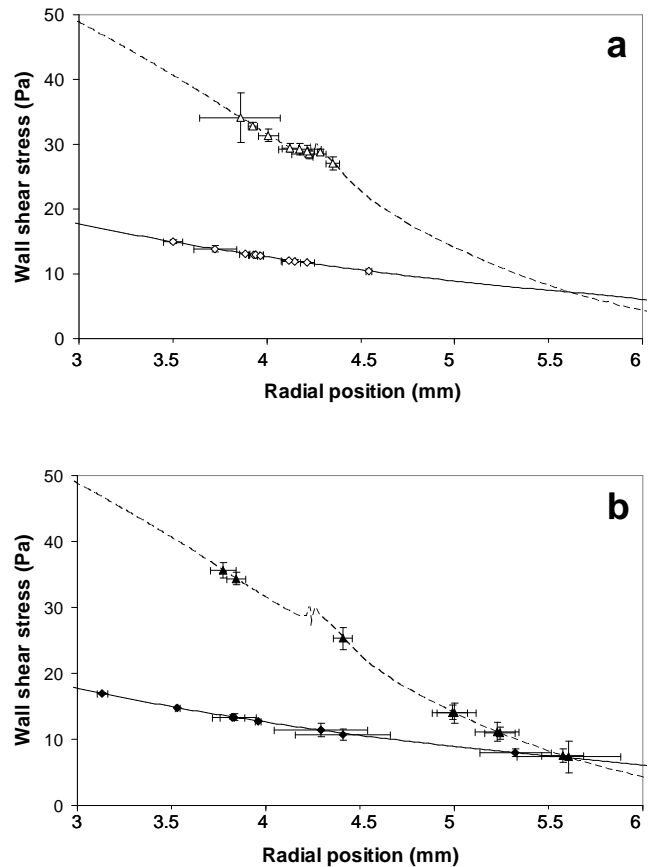


Fig. 7: Detachment radii measured (a) on oil-soiled polystyrene (open symbols) and, (b) on stainless steel (closed symbols) at 190 ml.min⁻¹ (♦) and 390 ml.min⁻¹ (▲) fitted to CFD-computed wall shear stress at 190 ml.min⁻¹ (—) and 390 ml.min⁻¹ (---).

the flow rate. The zone of good agreement corresponds to detachment radii > 3.5 mm at $190 \text{ ml}\cdot\text{min}^{-1}$ and > 4.5 mm at $390 \text{ ml}\cdot\text{min}^{-1}$.

From Figure 7, independently of the flow rate, the wall shear stress varies inversely with the detachment radius, as could have been expected. For stainless steel, the shear stress values are the same for long cleaning times and correspond to different detachment radii between the two flow rates. For polystyrene, the shear stress values computed at the two flow rates are however very different for similar detachment radii. At $390 \text{ ml}\cdot\text{min}^{-1}$, these wall shear stress values correspond to radial positions where the y^+ values predicted before mesh refinement were higher than 2 and where the wall shear stress curve presents irregularities due to the discontinuity in the y^+ distribution after mesh refinement.

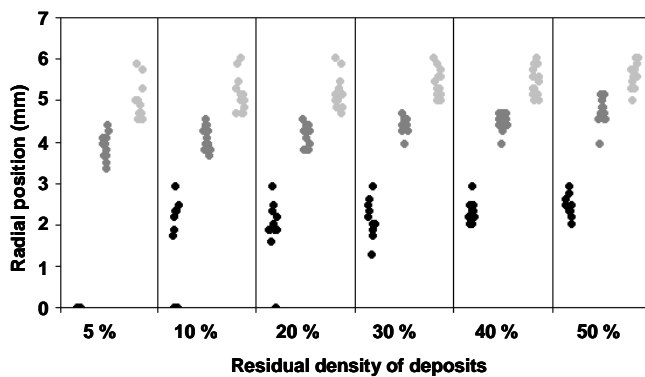


Fig. 8: Radial positions corresponding to different residual densities of starch deposits on starch-soiled polystyrene samples at 90 (●), 190 (●) or 390 (●) $\text{ml}\cdot\text{min}^{-1}$.

Starch granule aggregates

The radial positions measured on polystyrene surfaces are presented in Figure 8 as a function of the residual density of deposits (from 5 % to 50 % deposits remaining) for three flow rates. The corresponding wall shear stresses are presented in Figure 9.

As shown in Figure 8, the radial positions are well differentiated between the flow rates. At $90 \text{ ml}\cdot\text{min}^{-1}$, the residual density of deposits was always higher or equal to 10 %. When removal occurred, the variability of the measured radial positions was similar for all flow rates.

From Figure 9, it can be seen that the wall shear stresses computed by CFD are close and converging for a residual density of deposits of 50 %. The wall shear stress distribution was covering a much higher range at $390 \text{ ml}\cdot\text{min}^{-1}$ than at 90 and $190 \text{ ml}\cdot\text{min}^{-1}$. The mean wall shear stress values computed by CFD at $190 \text{ ml}\cdot\text{min}^{-1}$ are

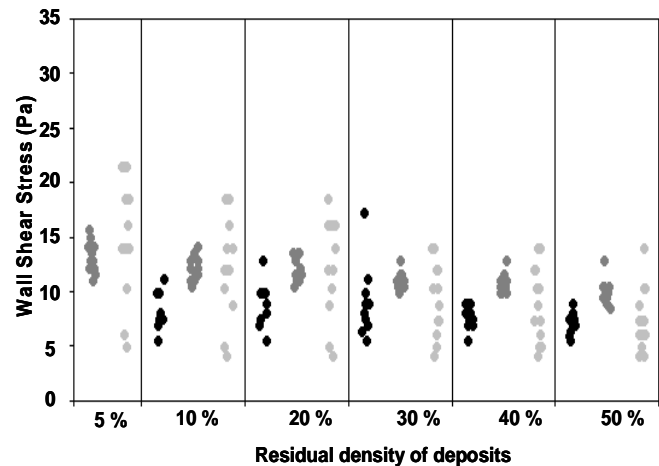


Fig. 9: Wall shear stresses computed by CFD for the radial positions of Figure 8 at 90 (●), 190 (●) or 390 (●) $\text{ml}\cdot\text{min}^{-1}$.

always about 3 Pa higher than the ones corresponding to the same residual deposits densities at $90 \text{ ml}\cdot\text{min}^{-1}$.

Based on Figures 8 and 9, if the experimental radial positions are plotted on the wall shear stress curves computed by CFD like it was presented for oil in Figure 7, two zones of consistency between the numerical solutions can be defined depending on the flow rate. The first one for radial positions comprised between about 3.1 and 5.7 mm and between 4.8 and 5.7 mm for the flow rates of 190 and $390 \text{ ml}\cdot\text{min}^{-1}$, respectively. The second one for radial positions comprised between about 2.0 and 3.0 mm and between 5.4 and 5.9 mm for the flow rates of 90 and $390 \text{ ml}\cdot\text{min}^{-1}$, respectively. The two zones of agreement correspond to wall shear stress values comprised between approximately 17.0 and 7.0 Pa ($190 - 390 \text{ ml}\cdot\text{min}^{-1}$) and 9.0 and 5.0 Pa ($90 - 390 \text{ ml}\cdot\text{min}^{-1}$).

At $390 \text{ ml}\cdot\text{min}^{-1}$, the wall shear stresses are high at radial positions smaller than 4.8 mm (18 – 22 Pa). Further, they become consistent with those computed at $190 \text{ ml}\cdot\text{min}^{-1}$ and then consistent with the ones computed at $90 \text{ ml}\cdot\text{min}^{-1}$ or even lower.

On stainless steel substrates, no starch deposit detachment was observed at 90 and $190 \text{ ml}\cdot\text{min}^{-1}$. At $390 \text{ ml}\cdot\text{min}^{-1}$, a first detachment radius was measured at 2.4 ± 0.4 mm for residual densities of deposits of 50 %, followed by a second cleaned zone, characterized by a lesser density of deposits and spreading from 4.9 ± 0.4 mm to 7.0 ± 0.8 mm (Figure 10).

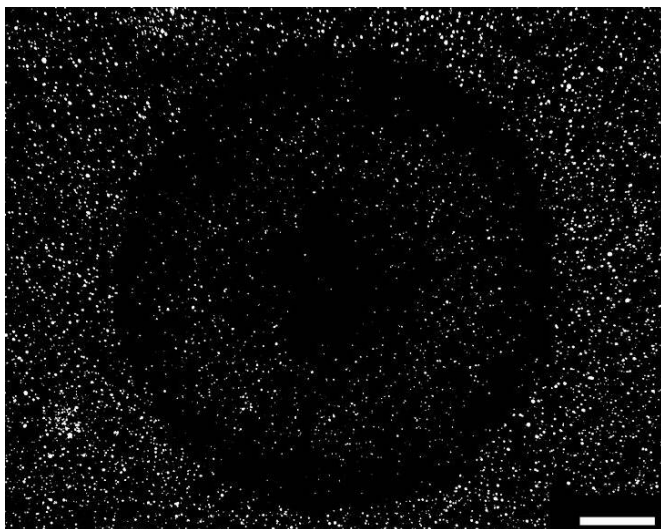


Fig. 10: Starch-soiled stainless steel surface submitted 5 min to a flow rate of $390 \text{ ml}\cdot\text{min}^{-1}$ in the RFC (Scale bar: 3 mm).

DISCUSSION

Evaluation of CFD computations from oil removal

As shown by the curves presented in Figure 6a, the results obtained by applying Eq. (3) give a wall shear stress decreasing with cleaning time and increasing radial positions, as expected from an ideal fully developed decelerating radial flow. Considering that the detachment radii were measured for the same soil on the same substrate, the wall shear stress values are not expected to differ by nearly a factor of 2 between the two flow rates.

When using the detachment radii from Figure 5 in Eq. (4), the experimental values of $Re_{modified}$ are then comprised between 1.1 and 4.5 ($190 \text{ ml}\cdot\text{min}^{-1}$) and between 2.4 and 9.6 ($390 \text{ ml}\cdot\text{min}^{-1}$) which are well above 0.25. Moreover, Jensen et al. (submitted) showed that the laminar CFD model used in the present study was only in good agreement with Eq. (3) for radial positions satisfying Eq. (4) over the whole range of Re_{inlet} investigated, suggesting that Eq. (4) is relevant in the present RFC. The curves presented in Figure 6a are thus not representative of experimental reality because Eq. (3) can only be used for an ideal fully developed decelerating radial flow, i.e. the radial positions satisfy the conditions of Eq. (4) (Fryer et al., 1985).

To fulfill the conditions of this last equation, the radial position should be at least 13 mm at $190 \text{ ml}\cdot\text{min}^{-1}$. This value is higher than the detachment radii reported in Figure 5, implying that the wall shear stress required to remove oil

from the substrates is too high to be computed by the analytical model proposed in the literature.

In agreement with this, Figure 6b shows that the wall shear stress values computed at $190 \text{ ml}\cdot\text{min}^{-1}$ by CFD for the experimental data are more than 10 times the values given by Eq. (3). Indeed, according to the computed flow pattern, all the experimental radial positions are situated under the primary recirculation zone of the RFC (Figure 4) where the flow lines are compressed at the vicinity of the lower wall (*vena contracta*). Higher wall shear stress values than the solution of Eq. (3) can thus be expected in the real RFC.

On stainless steel, the overlay of computed wall shear stress values at 190 and $390 \text{ ml}\cdot\text{min}^{-1}$ for cleaning periods longer than 3 min (Figure 6b) corresponds to detachment radii $> 3.5 \text{ mm}$ at $190 \text{ ml}\cdot\text{min}^{-1}$ and $> 4.5 \text{ mm}$ at $390 \text{ ml}\cdot\text{min}^{-1}$ (Figure 5). This suggests that the numerical wall shear stress is relevant at these radial positions and that it would also be the only factor influencing oil removal at such cleaning times. The growth of the detachment radius (Detry et al., 2007) and the decrease of the wall shear stress in the first minutes of cleaning on stainless steel at $390 \text{ ml}\cdot\text{min}^{-1}$, suggests that the mechanical action of the fluid is the main factor of the detachment process for short cleaning times. This is an interpretation supported by the fact that surfactants molecules generally need several minutes to saturate solid surfaces by adsorption (Brinck and Tiberg, 1996; Brinck et al., 1998; Geoffroy et al., 2000).

On polystyrene substrates, the wall shear stress values computed at $390 \text{ ml}\cdot\text{min}^{-1}$ are twice those at $190 \text{ ml}\cdot\text{min}^{-1}$ during the whole cleaning process. It can be seen from Figures 5 and 6b that those high differences in computed shear stresses correspond to small differences in measured radial positions. The spreading of oil drops is important on this substrate ($\theta_{oil} = 15^\circ$) and both the substrate and the soil are hydrophobic: the wall shear stress differences observed should thus be small and the mechanical action of the fluid should be the principal actor in the removal of oil droplets at both flow rates, as a consequence to the hindrance of the action of the surfactant (Boulangé-Petermann et al., 2006). If wall shear stress was the only factor controlling soil removal, the oil droplets should be removed by the same critical wall shear stress independently of the flow rate, as observed on stainless steel for long cleaning periods. The small change in detachment radius with the increase of the flow rate indicates, however, that oil is removed by the mechanical action of the fluid at higher shear stresses for higher flow rates, meaning that either the computation of the wall shear stress by CFD is wrong or, perhaps more likely, that other factors than wall shear stress influence the removal of the soil. This assumption is supported by the complexity of the flow close to the inlet and by the

observation of similar behavior with starch-soiled surfaces, as discussed further.

Concerning the cleanability of the oil-soiled surfaces, it is possible to conclude, based on both the detachment radius (Figure 5) and the wall shear stress curves (Figure 6b), that stainless steel is more cleanable than polystyrene.

Evaluation of CFD computations from starch removal

The conversion of the radial positions from Figure 8 into wall shear stress (Figure 9) points out a zone of good agreement between the laminar and the turbulent CFD-model for flow rates of 190 ml.min⁻¹ and 390 ml.min⁻¹. This zone, obtained for starch granules deposits removal, is identical to the one determined by oil removal experiments. Figure 9 shows that, for starch, the CFD models computed wall shear stress values converging for residual densities of deposits of 50%. This is a major improvement by comparison to the wall shear stress values given by Eq. (3) as shown for oil in Figure 6a. While the measured radial positions vary in a similar way for all flow rates, the variability of the wall shear stress values is comparable at 90 and 190 ml.min⁻¹ and much higher at 390 ml.min⁻¹. At this flow rate, the wall shear stress values vary on a broad range for small radial position variations, due to the higher slope of the CFD-computed wall shear stress curve (Figure 3).

This apparent deviating behavior with experimental data may be the sign of a weakness of the numerical solution at 390 ml.min⁻¹ due to the use of the SST k- ω model for transitional flows with y^+ values > 2 close to the inlet before mesh refinement and to the presence of irregularities in the wall shear stress distribution induced by refinement of the near wall cells following $y^+ < 1$ (Figure 7). Indeed, even if the k- ω model has proven itself superior to the k- ϵ model for the prediction of complex turbulent flows and quite effective in the recirculation regions of impinging jets (Park et al. 2003), it is also known to overestimate the wall shear stress while giving more realistic velocity profiles at the wall (Simpson, 1996). The SST k- ω model should be more accurate in terms of wall shear stress computation but it is nevertheless still possible that inaccuracies may be present in the solution in a simple geometry like the RFC, especially due to the particular nature of the flow in the equipment. In fact, a turbulent model was used but, according to Eq. (1), the flow undergoes a transition from turbulent to laminar as its direction changes from axial to radial in the inlet turn. The model may thus be more error-prone in computing the wall shear stress associated to the transitional regime in such geometry. It is also worthwhile to mention that the computed wall shear stresses were also varying more in the region close to the inlet during mesh refinement (Jensen et al., submitted).

The appearance of the annular pattern on starch-soiled stainless steel at 390 ml.min⁻¹ (Figure 10) is difficult to interpret. The presence of the first cleaned zone (at low radial positions) and its absence at lower inlet flow rates can be explained by the higher shear stresses required for soil removal that could not be reached at lower flow rates. The reason for the presence of the outer ring is however unknown. Nothing indicates any specific flow structure near the surface at these radial positions in the computed flow pattern. As the flow starts to expand after the *vena contracta* under the first recirculation zone at radial positions higher than 4.8 mm, the annular detachment of starch deposits might be the result of increased local wall shear stress fluctuations or of a boundary layer separation that may improve soil removal. The absence of more relevant experimental data prevents however the confirmation or undermining of any of these assumptions.

On starch-soiled polystyrene, the granules were less adhering and the annular pattern was not observed. It is nevertheless important to highlight that the detachment was always occurring in the zone corresponding to the annular pattern on stainless steel. This also shows that polystyrene is more cleanable than stainless steel toward starch granules (Figures 2 and 10).

In the case of starch deposits removal, the high variability of the computed wall shear stress values obtained for 390 ml.min⁻¹, can be the main explanation for the similarity between the values presented for that flow rate and for 90 and 190 ml.min⁻¹. At these last two flow rates, however, the distribution of the wall shear stress values was narrower and comparable to the repartition of the experimental radius measurements. This fact coupled with previous studies of the flow pattern in similar geometries (Armaly et al., 1983; Hsieh and Lin, 2005) seems to confirm the relevancy of the wall shear stress computations for the CFD laminar model.

Soil removal dependency on wall shear stress

The wall shear stress values required for starch removal at 190 ml.min⁻¹ are about 3 Pa higher than the ones corresponding to similar residual deposits densities at 90 ml.min⁻¹. This indicates that the application of a higher flow rate results in a higher shear stress required for soil removal. It may seem difficult to understand physically but similar behaviors have already been reported in impinging jets studies (Bundy et al., 2001; Bayouhd et al., 2005; Bouafsoun et al., 2006) where cells submitted to a laminar impinging flow during a short period (10 s or 30 s) were removed by higher wall shear stresses at higher flow rates. Bundy et al. (2001) assumed that the dependency of the wall

shear stress required for cell detachment on the flow rate was a consequence of the presence of different stress gradients at the radial positions having the same value of wall shear stress for different flow rates. Other parameters could also constitute part of the explanation like cell morphology, since the authors observed that rounder cells were more sensitive to the influence of the flow rate, viscoelastic effects related to the nature of the cell and normal pressure effects (Bundy et al., 2001). The above-mentioned studies concerned isolated mammalian cells or bacteria on various materials and for time intervals where the system could not reach equilibrium (Goldstein and DiMilla, 1997). Nevertheless, in the present study, the removal of the agglomerated starch granules may be influenced by similar factors as well.

In a flow system like the RFC or the impinging jet, where a sample can be submitted to various ranges of wall shear stress by simply modifying the disc spacing or the flow rate, soil removal from a solid surface is related to the wall shear stress. The present study, assuming that the CFD computations fit reality, suggests that the wall shear stress value required for soil removal may vary with the flow rate depending on the nature of the soil and on the spatial variation of other flow parameters in its vicinity. As a consequence, the value of the wall shear stress required for soil removal on a defined substrate may not be easily compared between different experimental setups.

CONCLUSIONS

The present study shows that the RFC can be used to characterize different materials concerning their cleanability and to generate useful information on the cleaning mechanisms of different soils.

Two CFD models were developed in order to establish the connection between experimental measurements performed in the RFC and wall shear stress values. The comparison of the numerical wall shear stresses corresponding to the experimental detachment radii measured at 90, 190 and 390 ml.min⁻¹ suggests that the laminar CFD model may give a reasonable estimation of the wall shear stress on the part of the flow domain situated under the primary recirculation zone and at radial positions where the flow is a fully developed decelerating flow. This was already supported by comparison of the laminar flow pattern with existing literature. At 390 ml.min⁻¹, good agreement with the laminar model was obtained for oil-soiled stainless steel surfaces. Nevertheless, the high variability of the computed wall shear stresses with the radial position and the unexplained presence of an annular pattern on starch-soiled stainless steel

substrates suggest that the computations still need improvement.

The assessment of the quality of CFD predictions at the wall in flow systems like the RFC can also be important to determine the most adequate model before transposing it on equipments of complex geometries or to model the flow and heat transfer conditions in part of equipments like plate and frame heat exchangers or welded plate heat exchangers.

Removal experiments performed with starch granules deposits suggested that the value of the wall shear stress required to remove a soil from a solid substrate may vary with the flow rate depending on the nature of the soil and on the spatial variation of other flow parameters in its vicinity.

Even if uncertainties exist about the relevance of computed wall shear stress values in parts of the flow domain, the use of CFD has been shown to be useful for the estimation of the flow pattern and of the wall shear stress distribution at the surface of a sample placed in a RFC under laminar flow regime. To improve the reliability of the computations, the effect of a possible azimuthal component of the velocity around the inlet axis (swirl) must be investigated and validation of the computations should be performed through flow visualization and/or velocimetry techniques.

ACKNOWLEDGEMENTS

This study has been financed by the Walloon Region (DGTRE) and the EU FP6 integrated project 'PathogenCombat' (FOOD-CT-2005-007081). Solange Mahiat is gratefully acknowledged for her technical assistance.

NOMENCLATURE

h	disk spacing, m
Q	inlet flow rate, m ³ s ⁻¹
r	radial position, m
r_i	inlet radius, m
Re_{inlet}	Reynolds number in the inlet pipe, dimensionless
Re_r	local Reynolds number, dimensionless
$Re_{modified}$	modified expression of Re_r , dimensionless
y^+	normalized distance of the first node point to the wall, dimensionless
μ	viscosity, Pa s
ρ	density, kg m ⁻³
τ	wall shear stress, Pa (N m ⁻²)

REFERENCES

- B. F. Armaly, F. Dust, J. C. F. Pereira and B. Schönung, 1983, Experimental and theoretical investigation of backward-facing step flow, *J. Fluid. Mech.*, Vol. 127, pp. 473-496.
- D.P. Bakker, H.J. Busscher and H.C. van der Mei, 2002, Bacterial Deposition in a Parallel Plate and Stagnation Point flow Chamber, *Microbiology*, Vol. 148, pp. 597 - 603.
- S. Bayouadh, L. Ponsonnet, H. Ben Ouada, A. Bakhrouf and A. Othmane, 2005, Bacterial detachment from hydrophilic and hydrophobic surfaces using a microjet impingement, *Colloid Surf. A-Physicochem. Eng. Asp.*, Vol. 266, pp. 160-167.
- C. J. P. Boonaert, Y. Dufrière and P. G. Rouxhet, 2002, Adhesion (primary) of microorganisms onto surfaces, in *Encyclopedia Environmental Microbiology*, ed. G. Bitton, Wiley, New York, pp. 113-132.
- A. Bouafoun, A. Othmane, A. Kerkeni, N. Jaffrézic and L. Ponsonnet, 2006, Evaluation of endothelial cell adherence onto collagen and fibronectin: A comparison between jet impingement and flow chamber techniques, *Materials Science and Engineering C*, Vol. 26, pp. 260-266.
- L. Boulangé-Petermann, C. Gabet, and B. Baroux, 2006, On the respective effect of the surface energy and micro-geometry in cleaning ability of bare and coated steels, *Colloid Surf. A-Physicochem. Eng. Asp.*, Vol. 272, pp. 56-62.
- J. Brinck, F. Tiberg, 1996, Adsorption Behavior of Two Binary Nonionic Surfactant Systems at the Silica-Water Interface, *Langmuir*, Vol. 12, pp. 5042-5047.
- J. Brinck, B. Jönsson, F. Tiberg, 1998, Kinetics of Nonionic Surfactant Adsorption and Desorption at the Silica-Water Interface: One Component, *Langmuir*, Vol. 14, pp. 1058-1071.
- K. J. Bundy, L. G. Harris, B. A. Rahn and R. G. Richards, 2001, Measurement of fibroblast and bacterial detachment from biomaterials using jet impingement, *Cell Biol. Int.*, Vol. 25, pp. 289-307.
- J. Detry, P. G. Rouxhet, L. Boulangé-Petermann, C. Deroanne and M. Sindic, 2007, Cleanability assessment of model solid surfaces with a radial-flow cell, *Colloid Surf. A-Physicochem. Eng. Asp.*, in press.
- P.J. Fryer, N. K. H. Slater and J. E. Duddridge, 1985, Suggestions for the Operation of Radial Flow Cells in Cell Adhesion and Biofouling Studies, *Biotechnol. Bioeng.*, Vol. 27, pp. 434-438.
- C. Geoffroy, M.A. Cohen Stuart, K. Wong, B. Cabane, V. Bergeron, 2000, Adsorption of Nonionic Surfactants onto Polystyrene: Kinetics and Reversibility, *Langmuir*, Vol. 16, pp. 6422-6430.
- A. Goldstein and P. A. DiMilla, 1997, Application of Fluid Mechanic and Kinetic Models to Characterize Mammalian Cell Detachment in a Radial-Flow Chamber, *Biotechnol. Bioeng.*, Vol. 55, pp. 616-629.
- J.C. Hsieh and T. F. Lin, 2005, Effects of jet-to-disk separation distance on the characteristics of mixed convective vortex flow in an impinging air jet confined in a cylindrical chamber, *Int. J. Heat Mass Transfer*, Vol. 48, pp. 511-525.
- B. B. B. Jensen, 2003, Hygienic Design of Closed Processing Equipment by use of Computational Fluid Dynamics. PhD Thesis, Technical University of Denmark, Denmark.
- B. B. B. Jensen and A. Friis, 2004, Critical wall shear stress for the EHEDG test method. *Chem. Eng. Process.*, Vol. 43, pp. 831-840.
- B. B. B. Jensen, J. Detry, C. Deroanne and M. Sindic, Laminar to turbulent flow in radial flow cell with aspect ratio of one, *Comput. Fluids*, submitted.
- A. Klavenes, T. Stalheim, O. Sjøvold, K. Josefsen and P. E. Granum, 2002, Attachment of *Bacillus cereus* spores with and without appendages to stainless steel surfaces, *Trans IChemE*, Vol. 80, pp. 312-318.
- P. S. Moller, 1963, Radial Flow without Swirl between Parallel Discs, *The Aeronautical Quarterly*, Vol. 14, pp. 163-186.
- T. H. Park, H. G. Choi, J. Y. Yoo and S. J. Kim, 2003, Streamline upwind numerical simulation of two-dimensional confined impinging slot jets, *Int. J. Heat Mass Transfer*, Vol. 46, pp. 251-262.
- R. L. Simpson, 1996, Aspect of turbulent boundary layer separation, *Prog. Aerospace Sci.*, 32, pp. 457-521.